Applied Catalysis B: Environmental 126 (2012) 153–160

Contents lists available at SciVerse ScienceDirect

Applied Catalysis B: Environmental

journal homepage: www.elsevier.com/locate/apcatb

Outstanding activity of sub-nm Au clusters for photocatalytic hydrogen production

Peichuan Shen[a], Shen Zhao[a], Dong Su[b], Yan Li[c], Alexander Orlov[a,*]

[a] Department of Materials Science and Engineering, Stony Brook University, Stony Brook, NY 11794, USA
[b] Center for Functional Nanomaterials, Brookhaven National Laboratory, Upton, NY 11973, USA
[c] Computational Science Center, Brookhaven National Laboratory, Upton, NY 11973, USA

ARTICLE INFO

Article history:
Received 2 April 2012
Received in revised form 13 July 2012
Accepted 20 July 2012
Available online 27 July 2012

Keywords:
Photocatalytic
Water splitting
Au clusters
Hydrogen production
Catalyst
TDDFT
CdS

ABSTRACT

Developing sustainable methods of hydrogen production can have significant environmental and energy efficiency benefits. A potentially viable way forward is to produce hydrogen from water by combining solar energy and heterogeneous catalysts. Our results indicate that sub-nm gold particles can provide an enormous enhancement in photocatalytic hydrogen production under visible light. We have observed a 35 times increase in activity for Au modified CdS as compared to that of unmodified catalyst. This activity was much higher than that of any other co-catalysts tested, which included 2–4 nm Pt, Ru, Pd and Rh nanoparticles modified CdS. The activity of sub-nm Au was also much better than that of CdS modified with larger Au particles. Our first-principles calculations of unsupported Au clusters indicated that there is a substantial difference in both shape and electronic properties between charged and neutral bare Au clusters as well as between bare and ligand-protected ones. This is the first ever demonstration of the remarkable potential of sub-nm Au particles for H_2 production.

1. Introduction

In order to reduce our dependence on fossil fuels it is vital to explore various sustainable energy options. For example, one possible strategy is to develop a hydrogen based energy economy, which can potentially offer numerous environmental and energy efficiency benefits [1]. However, the sustainable advantages of using hydrogen are limited given the fact that currently hydrogen is primarily produced from fossil fuels, such as natural gas, via steam reforming. Therefore, it will be tremendously beneficial to find alternative ways to produce hydrogen in efficient and sustainable manner. A potentially viable way forward is to make H_2 from water by combining solar energy and heterogeneous catalysts [2]. Following the discovery of water splitting by Fujishima and Honda [3], this topic has received a growing attention, especially in the recent years [4–6]. Some of the newly developed materials include various types of oxide, oxynitride and oxysulfide photocatalysts [7–10]. Although some of the photocatalysts can photocatalytically split water without a co-catalyst [11], most of them require loading of suitable co-catalysts to increase the hydrogen production rate.

It is believed that co-catalysts can lower activation energy for H_2 or O_2 evolution and serve as the active sites for H_2 or O_2 generation [6]. Metal oxides such as NiO, RuO_2 [12]; noble metals, such as Pt, Ru, Rh and Pd [13–16]; metal sulfides such as MoS_2 [17], WS_2 [18] as well as core-shell structures, such as Rh/Cr_2O_3 [19] were found to promote H_2 evolution. However, there are various issues related to these co-catalysts. For example, there are concerns about metal oxide co-catalysts long term stability [6]. At the same time, even though such noble metals as Pt, Pd, and Rh are excellent promoters for H_2 evolution, they can also facilitate water formation reaction (back reaction) from H_2 and O_2 [6,20], thus reducing the beneficial effects of their deposition. In contrast to the above mentioned co-catalysts, semiconductor surface modification with gold nanoparticles of approximately 20 nm in size has been shown to lead to a comparable (to Pt) activity for H_2 production with much lower rates of back reaction [21]. Utilizing even smaller Au particles can potentially bring some additional benefits. For example, there are reports indicating that Au nanoparticles loaded on TiO_2 [22,23] and perovskite titanate ($K_2La_2Ti_3O_{10}$) [24] can be promising photocatalysts for water splitting reactions. These reports were focused on the average Au particle size above 3 nm. However, exploring the sub-nm range of Au co-catalysts for water splitting has never been attempted before and photocatalytic properties of such materials are currently unknown.

Recently we have developed a modified synthetic procedure to produce sub-nm Au particles, which showed a significant activity for photocatalytic oxidation reactions of phenol in liquid phase and NO_2 in gas phase [25]. In order to explore the role of sub-nm

* Corresponding author. Tel.: +1 631 632 9978; fax: +1 631 632 8052.
E-mail address: aorlov@notes.cc.sunysb.edu (A. Orlov).

0926-3373/$ – see front matter © 2012 Elsevier B.V. All rights reserved.
http://dx.doi.org/10.1016/j.apcatb.2012.07.021

Au clusters in H_2 production we have chosen a standard catalyst (CdS), which is known to be active in water splitting, and modified it with sub-nm Au clusters. Given the CdS bandgap of 2.4 eV [26] and the positions of its valence and conductions bands, it has a modest activity for water splitting under visible light [14,27].

2. Experimental and computational methods

2.1. Catalyst preparation

CdS nanoparticles were prepared by the following method. A solution of sodium sulfide (Na_2S) was added to cadmium acetate solution ($Cd(CH_3COO)_2{\cdot}2H_2O$) by using a syringe pump (the injection speed of 0.2 ml/min) under vigorous stirring. The molar ratios were 1:1 and the mixture was stirred for 24 h. Then the resulting sample was centrifuged, washed with deionized water for 3 times, dried at 60 °C overnight and calcined at 400 °C for 45 min.

Sub-nm gold particles synthesis was based on the following approach. $Au(PPh_3)Cl$ was dissolved in $CHCl_3$ to reach a final concentration of 10^{-3} mol/l. About 10^{-3} mol/l $P(Ph)_2(CH_2)_4P(Ph)_2$ was subsequently added to the mixture to achieve the target cluster size. Finally, 5×10^{-3} mol/l of the reducing agent (aborane–tert-butylamine complex) was added under continuous stirring for 24 h at room temperature.

To modify CdS surface with nanoparticles, about 200 mg of CdS was added to 20 ml of dichloromethane, followed by addition of Au nanoparticles (NPs) precursors. The gold deposition procedure on CdS powders was achieved by varying the ratios of CdS and AuNPs precursors developed in the previous step. The mixture was stirred overnight, followed by thermal activation (150 °C, 2 h) in vacuo. The final powder was then washed with acetone.

Different noble metals, including Au, Pt, Ru, Pd and Rh, were loaded on CdS by photodeposition method using $HAuCl_4$, $H_2PtCl_6{\cdot}6H_2O$, $RuCl_3$, $PdCl_2$ and $RhCl_3$ aqueous solutions, respectively.

2.2. Techniques of characterization

UV–Vis optical absorption spectrum of unsupported Au clusters was obtained by Ultraviolet–visible spectroscopy (Thermo Evolution 3000). Transmission electron microscopy (TEM) images were obtained using a JEOL2100F (200 kV) microscope. Scanning transmission electron microscopy (STEM) imaging was carried out in the Center for Functional Nanomaterials at Brookhaven National Lab, using a Hitachi HD2700C (200 kV) with a probe aberration-corrector. We have used an electron probe of 1.3 Å at a semi-collection angle between 114 and 608 mrad.

2.3. Catalytic reactions

Photocatalytic reactions were carried out in a customized Pyrex reactor connected to a closed gas circulation and evacuation system. 100 mg of catalyst was suspended in 200 ml of aqueous solution containing 0.25 M Na_2S and 0.35 M Na_2SO_3, which acted as sacrificial reagent [28]. The suspension was put in the dark and purged with argon while being stirred by magnetic stir bar for 30 min, which was followed by degassing procedure. 40 Torr argon was introduced into the system as carrier gas. Then the suspension was irradiated by a 300 W Xe lamp (Newport, Model 66984) equipped with an optical cutoff filter ($\lambda > 420$ nm, L42, Hoya) to eliminate ultraviolet light and a 10 cm water filter ($\lambda < 800$ nm) to eliminate IR. The amount of H_2 produced was analyzed using an online gas chromatography unit (Agilent 7890A) equipped with a thermal conductivity detector and a 5 Å molecular sieve column.

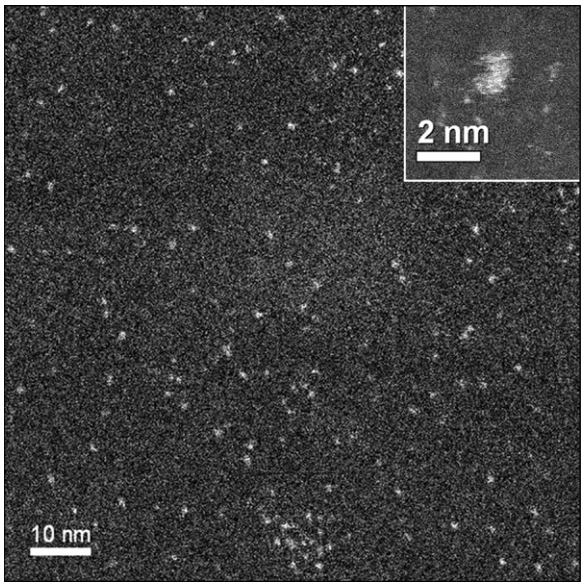

Fig. 1. STEM image of unsupported Au clusters. Insert shows higher resolution image of sub-nm Au cluster.

2.4. Computational procedures

First principles density functional theory (DFT) and time-dependent density functional theory (TDDFT) calculations for unsupported Au nanoparticles were carried out with the Quantum Espresso [29] package, using norm-conserving pseudopotentials, PBE [30] exchange-correlation functional and plane-wave basis sets with a kinetic energy cutoff of 50 Ry. A simple cubic supercell of 50 bohr and the Martyna–Tuckerman corrections [31] were applied for both neutral and charged gold nanoparticles. The structure of Au nanoclusters identified in the mass spectrum were simplified by replacing each diphosphine ligand $L = P(Ph)_2(CH_2)_4P(Ph)_2$ with two PH_3 groups. In particularly, we have studied in detail the $[Au_9(PH_3)_6Cl_2]^+$ and $[Au_{11}(PH_3)_{68}]^+$ nanoparticles.

3. Results and discussion

3.1. Characterization of sub-nm Au and Au/CdS

In order to understand the role of Au particle size in photocatalytic activity, we have conducted a detailed characterization of both supported and unsupported Au samples using STEM, TEM and UV–Vis spectroscopy. Figs. 1 and 2 and the previous work on unsupported clusters [25] indicated that the average particle size of unsupported Au was about 0.8 ± 0.1 nm as determined by STEM, which can be attributed to abundance of Au_{11}–Au_{13} clusters [32,33]. We also found [25] that the precursor solution contained both single atoms and clusters up to 11–13 gold atoms in size, as determined by matrix-assisted laser desorption/ionization-time of flight mass spectrometer (MALDI-TOF) measurements [25]. A detailed analysis of UV–Vis data of unsupported Au clusters showed a prominent peak at 410 nm. Fig. 3 shows the computed optical spectrum for mixed ligand protected $Au_{11}{}^+$ and $Au_9{}^+$ clusters, with two dominating peaks at 420 nm and 300 nm, in reasonable agreement with UV–Vis data. A close inspection of the corresponding excitations show significant Au 5d → 6sp transition characters and metal-to-ligand charge transfer transition characters, respectively. Our DFT calculations of unsupported Au clusters indicated that there is a substantial difference in both shape and electronic properties between charged and neutral bare Au clusters as well as between bare and ligand-protected ones, as shown in Fig. 4, which

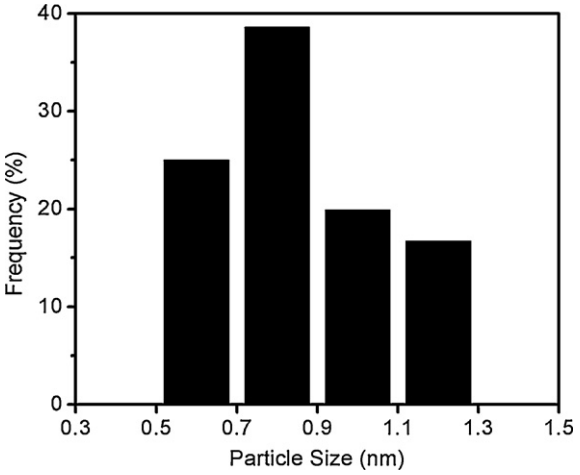

Fig. 2. Particle size distribution of unsupported sub-nm Au with average Au size of about 0.8 ± 0.1 nm.

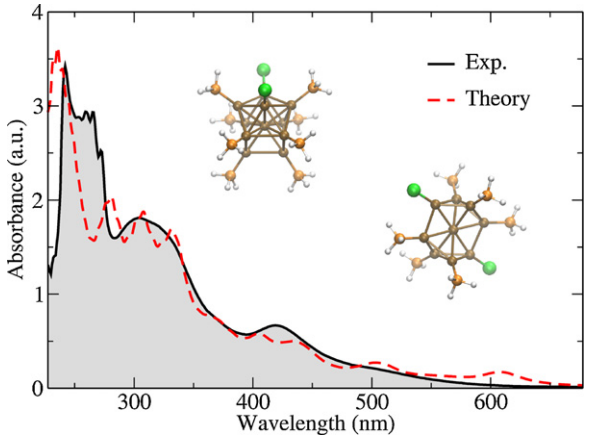

Fig. 3. Computed optical spectrum of mixed $[Au_9(PH_3)_6Cl_2]^+$ and $[Au_{11}(PH_3)_8Cl_2]^+$ nanoclusters, in comparison with measured UV–Vis spectrum.

might affect the shape of supported co-catalysts. For example, the minimum energy structure of the bare Au_{11}^- cluster is planar with a computed gap of 1.0 eV, while that of Au_{11}^+ is three-dimensional with a DFT gap of 1.7 eV (see Figs. 3 and 4). Additionally the density of states of deprotected Au clusters indicate the appearance of HOMO–LUMO gap of about 2 eV (Au_{11}^+), as shown in Fig. 5, which can affect the charge transfer from photoexcited CdS to Au. All these factors might need to be taken into account to explain the extraordinary activity of sub-nm Au clusters discovered in our work.

Fig. 6 shows the STEM-high angle annular dark field (HAADF) image of 5 wt.% Au/CdS. Fig. 7 confirms that the average particle size of the samples was around 0.95 ± 0.1 nm. The Au particle size distribution in the sample indicated that only minor agglomeration of Au clusters has occurred after their deposition and de-protection as compared to unsupported clusters. Moreover, in order to explore particle stabilities, we subjected our samples to different thermal activation temperatures ranging from 130 °C to 180 °C. However, we did not observe any detectable changes in terms of particle sizes.

3.2. Catalytic results

Fig. 8 shows the rates of H_2 evolution on sub-nm Au/CdS with different amounts of Au loadings. The results indicated that sub-nm gold particles can provide an enormous improvement in photocatalytic H_2 production under visible light. For comparison, the rate of H_2 evolution on pure CdS is also plotted. As expected, unmodified CdS photocatalyst exhibited very low photocatalytic activity for H_2 evolution (ca. 12 μmmol h^{-1}), which is consistent with the

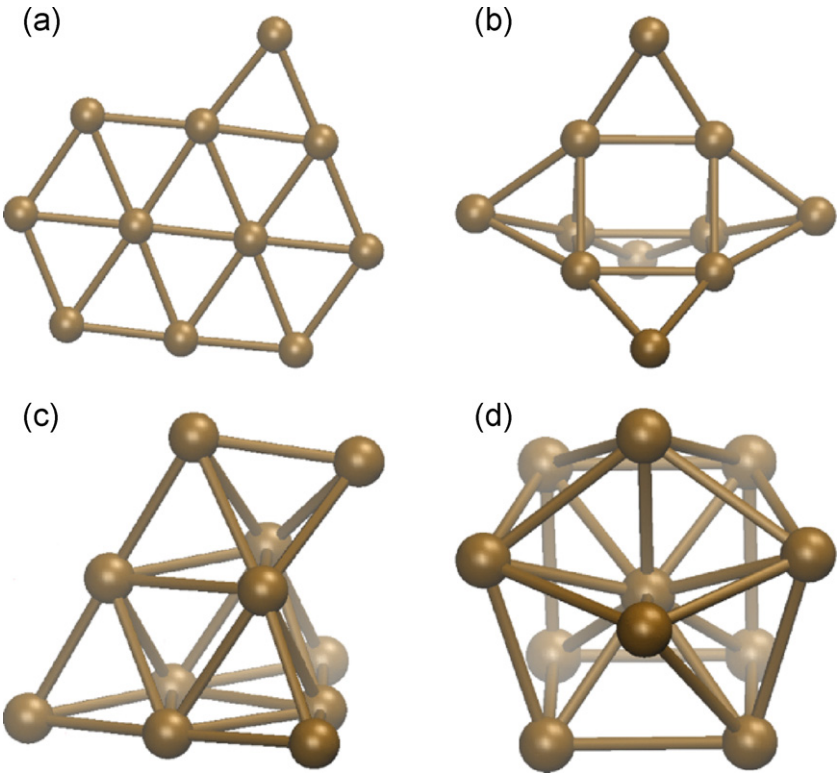

Fig. 4. DFT-optimized geometries of Au clusters: (a) bare Au_{11}^- and Au_{11}^0, (b) bare Au_{11}^+, (c) bare Au_{11}^{3+} and (d) $[Au_{11}(PH_3)_8Cl_2]^+$ and $[Au_{11}(PH_3)_{10}]^{3+}$ (only Au atoms are shown).

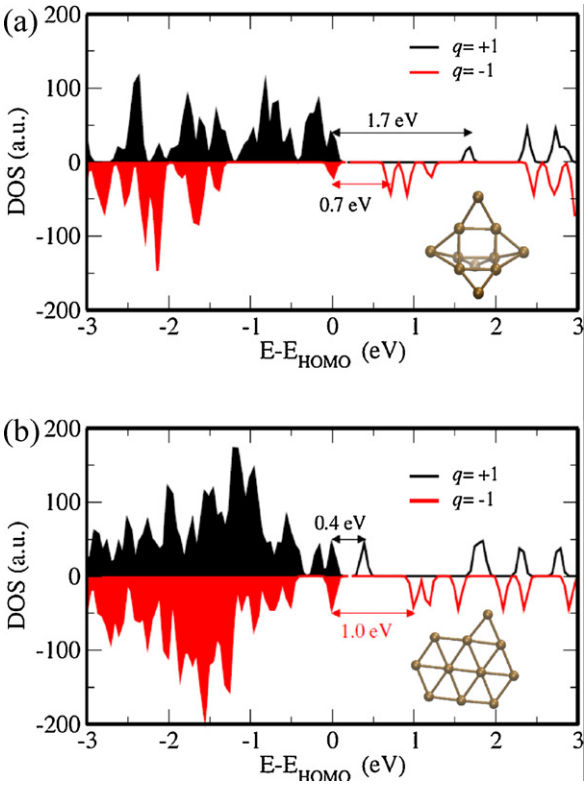

Fig. 5. Computed density of states (DOS) of bare Au_{11} clusters: (a) Au_{11}^{+} (3D, gap = 1.7 eV) and (b) Au_{11}^{-} (2D, gap = 1.0 eV). For comparison, DOS of the same clusters but with opposite charges, i.e. 3D Au_{11}^{-} (gap = 0.7 eV) and 2D Au_{11}^{+} (gap = 0.4 eV), are also presented.

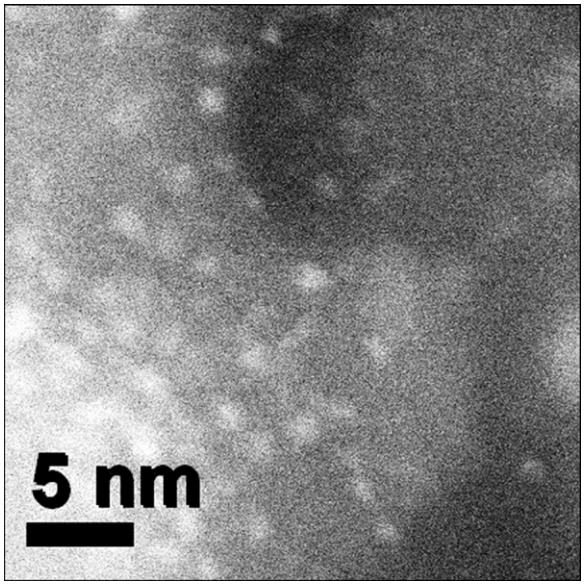

Fig. 6. Scanning transmission electron micrograph of 5 wt.% sub-nm Au loaded on CdS.

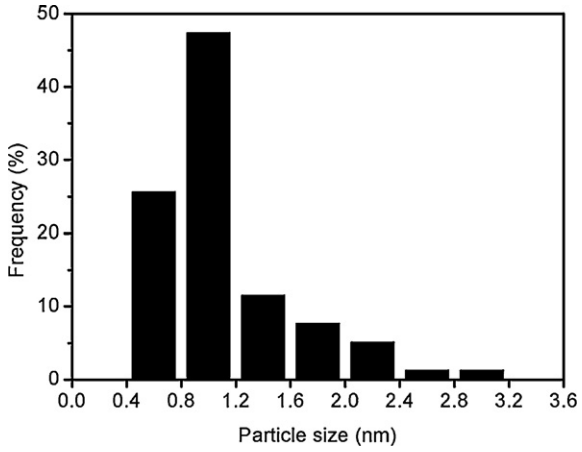

Fig. 7. Particle size distribution of sub-nm Au loaded on CdS with average Au size of about 0.95 ± 0.1 nm (particle size distribution is based on several STEM images).

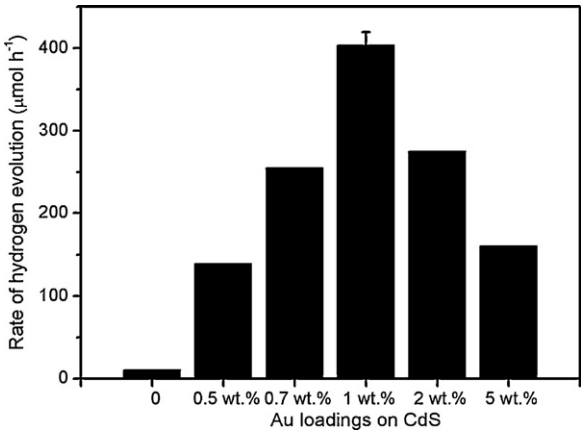

Fig. 8. Rates of H_2 evolution on sub-nm Au/CdS with different amounts of Au loadings.

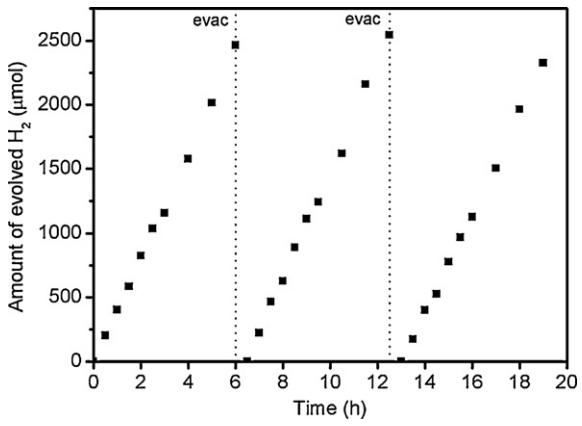

Fig. 9. Stability test for 1 wt.% sub-nm Au/CdS.

previously published reports [14,17]. In contrast to unsupported CdS, sub-nm Au modified photocatalysts exhibited a remarkably improved activity even at very low gold loadings. The most active catalyst was 1 wt.% Au modified CdS, which showed about 35 times improvement in H_2 production rate (ca. 404 μmol h^{-1}) as compared to that of unmodified CdS. We have repeated the experiment 3 times to confirm this very significant result (as indicated by the error bars in Fig. 8). A further increase in Au loading resulted in decrease in photocatalytic activity, probably due to reduction of illuminated area of CdS (due to Au coverage) and potential agglomeration of sub-nm Au clusters. Fig. 9 shows H_2 evolution as a function of time for the most active sub-nm Au/CdS sample, where we cycled this catalyst 3 times to determine its stability and reactivity. The sample showed almost linear concentration dependence for all 3 cycles. Even after 18 h of reaction there was no significant deactivation of the catalyst. The robustness in catalytic performance can be attributed to stability of both sub-nm Au clusters and CdS.

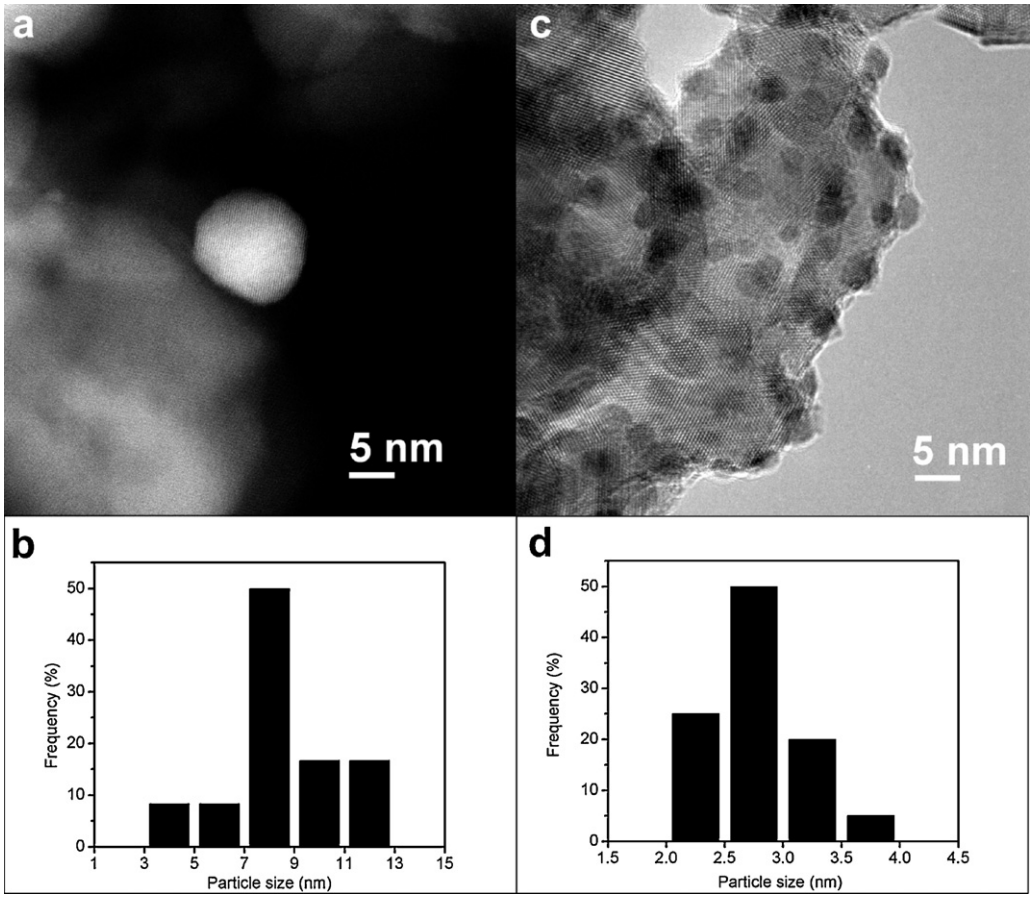

Fig. 10. STEM image and particle size distribution of Au/CdS sample with different Au sizes. (a) STEM image showing 9 nm Au loaded on CdS. (b) Particle size distribution of 9 nm Au nanoparticles, average size = 9.0 ± 0.3 nm (particle size distribution is based on several STEM images). (c) TEM image showing 3 nm Au loaded on CdS. (b) Particle size distribution of 3 nm Au nanoparticles, average size = 3.0 ± 0.1 nm (particle size distribution is based on several TEM images).

Under normal conditions, CdS tends to undergo photo-corrosion [34], however, the presence of sacrificial reagents (Na_2SO_3 and Na_2S) can significantly slow this process [4].

One important question is whether the activity of small Au clusters is different from that of larger particles. In order to address this question we subjected the most active sample (1 wt.% sub-nm Au/CdS) to heat treatment, which resulted in Au agglomeration as indicated by our STEM results. Fig. 10a shows the STEM image of this sample after the heat treatment. The average Au particle size of heat-treated catalyst was about 9.0 ± 0.3 nm, as shown in Fig. 10b. In order to gain even better understanding of the size dependent catalytic activity, we used photodeposition method to produce intermediate size Au particles. Fig. 10c shows the TEM image of Au particles prepared by photodeposition method, where the average Au particle size achieved by this method was 3.0 ± 0.1 nm (Fig. 10d). Fig. 11 shows activity of CdS samples modified with Au nanoparticles of difference sizes. It is apparent that sub-nm Au modified CdS had about 11 times higher activity than that of the sample modified with 9 nm Au. The photocatalytic activity of sample modified with 3 nm Au was found to be comparable to that of 9 nm Au sample, confirming that sub-nm particles are indeed unique in their remarkable behavior. To confirm that Au nanoparticles themselves did not exhibit a photocatalytic activity, sub-nm Au particles (1 wt.%) were deposited on SiO_2, which is known to be inactive for water splitting reaction. No hydrogen evolution was observed for Au/SiO_2 composite catalyst. Although for larger metal particles a correlation between perimeter/surface area of metal nanoparticles and activity has been proposed [35,36], that was done for larger particles exhibiting metallic properties. In our case, following the overly simplistic method used by Bowker [37] used for larger particles, the total perimeter of all sub-nm Au particles for the same Au loading was around 80 times longer than that of 9 nm Au, while the total surface area of sub-nm Au was around 9 times higher than that of 9 nm Au. However, the fact that activity of 3 nm Au particles

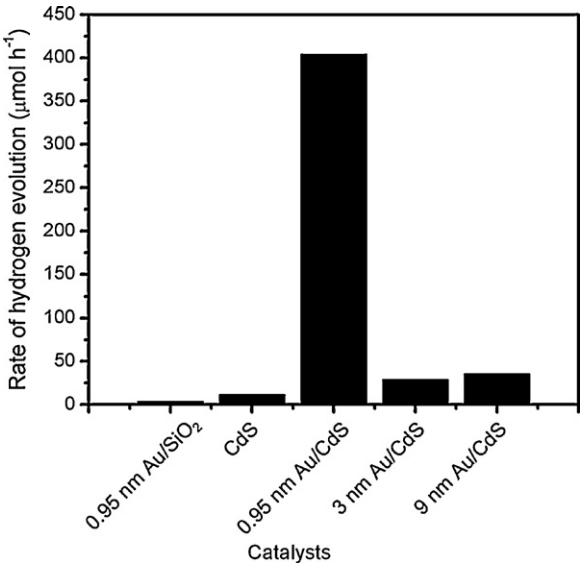

Fig. 11. Hydrogen evolution rates for Au/CdS with different sizes of Au nanoparticles.

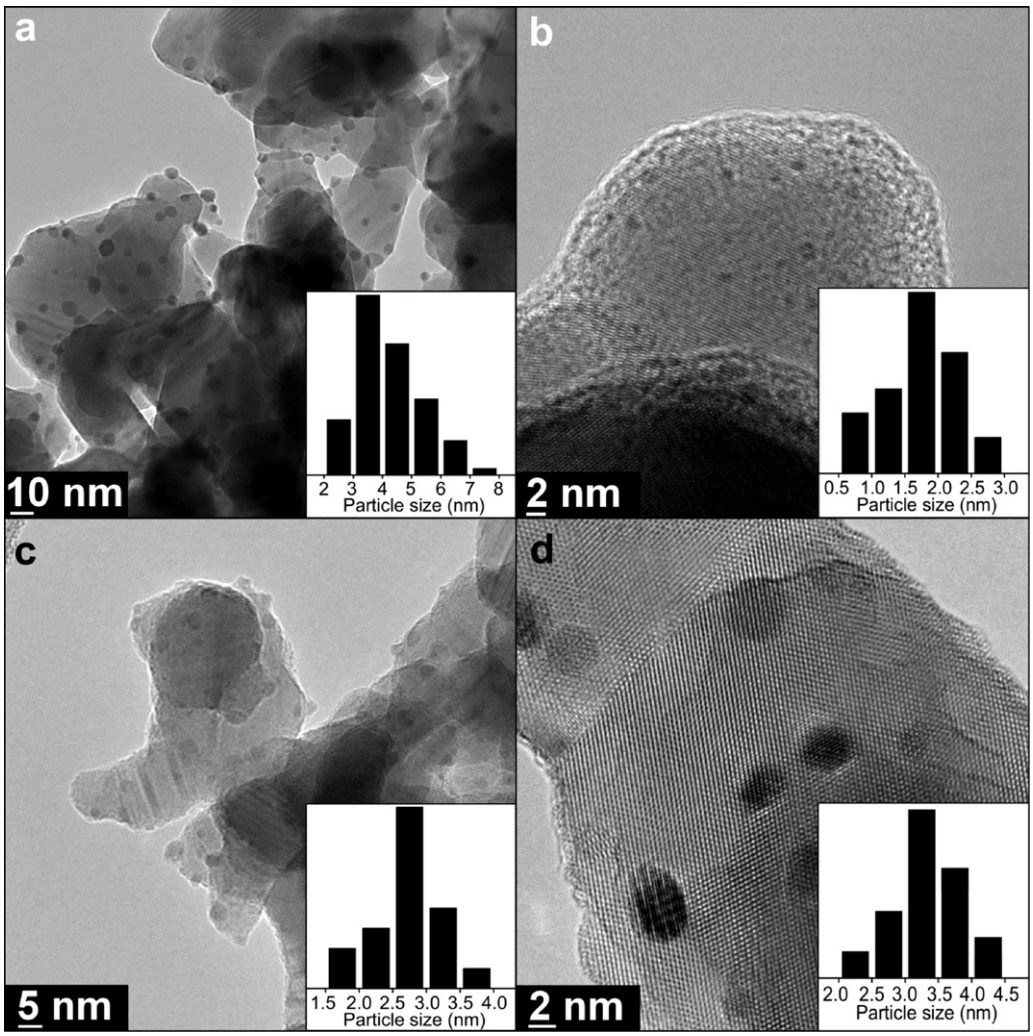

Fig. 12. TEM images of (a) Pt/CdS, (b) Ru/CdS, (c) Pd/CdS and (d) Rh/CdS. The inserts show the particle size distributions of Pt (average particle size = 3.7 nm), Ru (average particle size = 2.0 nm), Pd (average particle size = 3.2 nm) and Rh (average particle size = 3.6 nm), respectively.

was almost the same as that of 9 nm particles shows that a simple correlation between surface area and/or perimeter might not be relevant in our case.

Finally, to compare the activity of sub-nm Au with other co-catalysts, we have prepared CdS loaded with other noble metal co-catalysts. These included Pt, Ru, Pd and Rh modified CdS, where we kept a comparable co-catalyst loading (1 wt.%), which was also similar to the loading of the most active Au/CdS sample. As indicated earlier, the above-mentioned co-catalysts are known to promote H_2 evolution. To prepare these composite materials, we employed the same photodeposition method as the one we used to produce 3 nm Au nanoparticles modified CdS described above. Fig. 12 shows TEM characterizations and particle size distributions of Pt/CdS, Ru/CdS, Pd/CdS and Rh/CdS samples. The average particle size of loaded co-catalysts ranged between 2.0 and 3.7 nm. A comparison of H_2 evolution rates between these catalysts and 3 nm Au modified CdS showed that the activity of 3 nm Au was better than that of Pd/CdS and Rh/CdS, while Au/CdS activity being somewhat worse than that of Pt/CdS and Ru/CdS (Fig. 13). A careful examination of CdS particle sizes for the above mentioned catalysts indicated that the CdS particle size remained the same despite undergoing various nanoparticles deposition, heat treatment and washing procedures. This indicates the differences in catalytic behavior can be primarily attributed to co-catalysts.

The reason for striking photocatalytic activity of sub-nm co-catalysts is currently unknown, given a surprising absence of relevant literature on Au_{11} catalytic activity. For example, the observations of Au_3–Au_{11} electrocatalytic activity for O_2 reduction do not have a significant relevance to this study [38]. Moreover, the known charge separation properties of larger Au nanoparticles

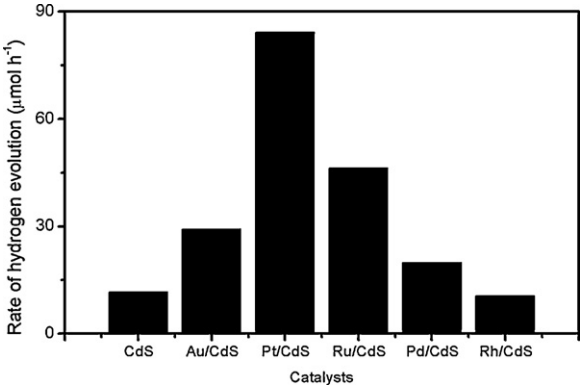

Fig. 13. Rates of hydrogen production from different noble metal co-catalysts loaded on CdS. The average particle size of Au, Pt, Ru, Pd and Rh was 3.0 nm, 3.7 nm, 2.0 nm, 3.2 nm and 3.6 nm, respectively.

in composite Au/CdS systems [39,40] cannot be used to approximate the behavior of sub-nm Au particles described in this work, given the appearance of HOMO–LUMO gap for sub-nm particles. Although size-dependent shifts in the Fermi level were observed for Au nanoparticle deposited on TiO_2, where the transient absorption measurements were done for the Au particles sizes down to 5 nm [41,42], this mechanism of enhancement can only partially account for enhancement of H_2 evolution of 3 nm Au modified CdS described in this paper and might not be applicable for smaller particles. The effects of localized surface plasmon resonance (LSPR) for larger Au particles have been discussed in the literature, however, the role of this mechanisms in catalytic activity of sub-nm clusters is unclear, given that such clusters are not metallic [43]. It is crucial to mention that both shape and electronic structure of supported Au particles can have profound effect on their catalytic activity. A charge on Au clusters can affect the work function of CdS surface and charge transfer mechanisms, ultimately affecting the overall activity for hydrogen production. The research on plasmon resonance in Au/CdS colloidal nanocomposites showed that the key optoelectronic properties of composite heterostructures comprising electrically coupled metal and semiconductor domains are significantly different from those weak interdomain coupling systems [44]. It was indicated the quantum confinement of CdS was effectively decreased by charging of gold domains under illumination. Shape is also an important fact which contributes to the photocatalytic activity. The studies indicating a correlation between supported Au particle shape (2D and 3D) and particle charge were done on a limited number of oxides and they might not be directly applicable for the gold–metal sulfide composite semiconductor described here [45,46]. Also, there are several studies on significant catalytic activity of 2D gold clusters due to presence of low coordinated Au atoms [47,48] and our calculations described above indeed indicate a feasibility of both 2D and 3D geometry of the unsupported clusters. However, the importance of this phenomenon in photocatalysis needs further investigation, given that the published studies were not conducted for light-activated catalytic reactions. In order to clarify the remarkable activity of small Au nanoparticles, work is currently underway to investigate the energy level alignment and possible charge transfer process at the interface of deprotected Au nanoparticles and the CdS substrate. Moreover, additional experiments to explore photocatalytic properties of other metals synthesized in sub-nm form, for example, sub-nm Pt and sub-nm Pd, are currently in progress.

4. Conclusion

In this work we have shown that the rate of H_2 evolution on CdS can be dramatically enhanced by sub-nm Au particles. The activity of CdS was increased by up to 35 times when loaded with 1 wt.% sub-nm Au. This activity was much higher than that of any other co-catalysts tested. It appears that this extraordinary activity enhancement is related to sub-nm dimensions of Au particles, as larger Au particles had much lower activity. We believe that the strategy of modifying semiconductor surfaces with Au to increase H_2 production rate is not limited to CdS surfaces and can be extended to other semiconductor photocatalysts.

Acknowledgments

This research has been supported by the NSF CBET Award 1152732. The calculations were performed at the NERSC facilities. The work of DS and YL was supported by Brookhaven Science Associates, LLC under Contract No. DE-AC02-98CH10886 with the U.S. Department of Energy.

References

[1] T. Bak, J. Nowotny, M. Rekas, C.C. Sorrell, International Journal of Hydrogen Energy 27 (2002) 991–1022.
[2] N.Z. Muradov, T.N. Veziroglu, International Journal of Hydrogen Energy 33 (2008) 6804–6839.
[3] A. Fujishima, K. Honda, Nature 238 (1972) 37.
[4] A. Kudo, Y. Miseki, Chemical Society Reviews 38 (2009) 253–278.
[5] K. Maeda, K. Teramura, D.L. Lu, T. Takata, N. Saito, Y. Inoue, K. Domen, Nature 440 (2006) 295.
[6] K. Maeda, K. Domen, Journal of Physical and Chemical Letters 1 (2010) 2655–2661.
[7] W. Yao, H. Iwai, J. Ye, Dalton Transactions (2008) 1426–1430.
[8] R. Abe, T. Takata, H. Sugihara, K. Domen, Chemical Communications (2005) 3829–3831.
[9] Y. Lee, H. Terashima, Y. Shimodaira, K. Teramura, M. Hara, H. Kobayashi, K. Domen, M. Yashima, Journal of Physical Chemistry C 111 (2007) 1042–1048.
[10] Z.B. Lei, G.J. Ma, M.Y. Liu, W.S. You, H.J. Yan, G.P. Wu, T. Takata, M. Hara, K. Domen, C. Li, Journal of Catalysis 237 (2006) 322–329.
[11] H. Kato, A. Kudo, Journal of Physical Chemistry B 105 (2001) 4285–4292.
[12] Z.G. Zou, J.H. Ye, K. Sayama, H. Arakawa, Nature 414 (2001) 625–627.
[13] H.G. Kim, D.W. Hwang, J.S. Lee, Journal of the American Chemical Society 126 (2004) 8912–8913.
[14] H. Park, W. Choi, M.R. Hoffmann, Journal of Materials Chemistry 18 (2008) 2379–2385.
[15] I. Tsuji, H. Kato, A. Kudo, Angewandte Chemie International Edition 44 (2005) 3565–3568.
[16] H. Kaga, K. Saito, A. Kudo, Chemical Communications 46 (2010) 3779–3781.
[17] X. Zong, H.J. Yan, G.P. Wu, G.J. Ma, F.Y. Wen, L. Wang, C. Li, Journal of the American Chemical Society 130 (2008) 7176.
[18] C. Li, X. Zong, J.F. Han, G.J. Ma, H.J. Yan, G.P. Wu, Journal of Physical Chemistry C 115 (2011) 12202–12208.
[19] K. Maeda, K. Teramura, D.L. Lu, N. Saito, Y. Inoue, K. Domen, Journal of Physical Chemistry C 111 (2007) 7554–7560.
[20] K. Maeda, K. Teramura, D.L. Lu, N. Saito, Y. Inoue, K. Domen, Angewandte Chemie International Edition 45 (2006) 7806–7809.
[21] A. Iwase, H. Kato, A. Kudo, Catalysis Letters 108 (2006) 6–9.
[22] G.L. Chiarello, L. Forni, E. Selli, Catalysis Today 144 (2009) 69–74.
[23] O. Rosseler, M.V. Shankar, M.K.L. Du, L. Schmidlin, N. Keller, V. Keller, Journal of Catalysis 269 (2010) 179–190.
[24] Y.W. Tai, J.S. Chen, C.C. Yang, B.Z. Wan, Catalysis Today 97 (2004) 95–101.
[25] S. Zhao, G. Ramakrishnan, D. Su, R. Rieger, A. Koller, A. Orlov, Applied Catalysis B 104 (2011) 239–244.
[26] Y.X. Yin, Z.G. Jin, F. Hou, Nanotechnology 18 (2007).
[27] N.Z. Bao, L.M. Shen, T. Takata, K. Domen, Chemistry of Materials 20 (2008) 110–117.
[28] A.J. Frank, K. Honda, Journal of Physical Chemistry 86 (1982) 1933–1935.
[29] P. Giannozzi, S. Baroni, N. Bonini, M. Calandra, R. Car, C. Cavazzoni, D. Ceresoli, G.L. Chiarotti, M. Cococcioni, I. Dabo, A. Dal Corso, S. de Gironcoli, S. Fabris, G. Fratesi, R. Gebauer, U. Gerstmann, C. Gougoussis, A. Kokalj, M. Lazzeri, L. Martin-Samos, N. Marzari, F. Mauri, R. Mazzarello, S. Paolini, A. Pasquarello, L. Paulatto, C. Sbraccia, S. Scandolo, G. Sclauzero, A.P. Seitsonen, A. Smogunov, P. Umari, R.M. Wentzcovitch, Journal of Physics-Condensed Matter 21 (2009).
[30] J.P. Perdew, K. Burke, M. Ernzerhof, Physical Review Letters 77 (1996) 3865–3868.
[31] G.J. Martyna, M.E. Tuckerman, Journal of Chemical Physics 110 (1999) 2810–2821.
[32] M.F. Bertino, Z.M. Sun, R. Zhang, L.S. Wang, Journal of Physical Chemistry B 110 (2006) 21416–21418.
[33] J.C. Idrobo, W. Walkosz, S.F. Yip, S. Ogut, J. Wang, J. Jellinek, Physical Reviews B 76 (2007).
[34] D. Meissner, R. Memming, B. Kastening, Journal of Physical Chemistry 92 (1988) 3476–3483.
[35] G.P. Wu, T. Chen, W.G. Su, G.H. Zhou, X. Zong, Z.B. Lei, C. Li, International Journal of Hydrogen Energy 33 (2008) 1243–1251.
[36] P.K. He, J.J. Yang, D.M. Xang, X.H. Wang, M. Zhang, Chinese Journal of Catalysis 27 (2006) 71–74.
[37] M. Bowker, D. James, P. Stone, R. Bennett, N. Perkins, L. Millard, J. Greaves, A. Dickinson, Journal of Catalysis 217 (2003) 427–433.
[38] M.J. Rodriguez-Vazquez, M.C. Blanco, R. Lourido, C. Vazquez-Vazquez, E. Pastor, G.A. Planes, J. Rivas, M.A. Lopez-Quintela, Langmuir: The ACS Journal of Surfaces and Colloids 24 (2008) 12690–12694.
[39] W.-W. Zhao, J. Wang, J.-J. Xu, H.-Y. Chen, Chemical Communications 47 (2011) 10990–10992.
[40] W.-T. Chen, T.-T. Yang, Y.-J. Hsu, Chemistry of Materials 20 (2008) 7204–7206.
[41] V. Subramanian, E.E. Wolf, P.V. Kamat, Journal of the American Chemical Society 126 (2004) 4943–4950.
[42] B.Z. Tian, J.L. Zhang, T.Z. Tong, F. Chen, Applied Catalysis B 79 (2008) 394–401.
[43] T. Torimoto, H. Horibe, T. Kameyama, K. Okazaki, S. Ikeda, M. Matsumura, A. Ishikawa, H. Ishihara, Journal of Physical and Chemical Letters 2 (2011) 2057–2062.

[44] E. Khon, A. Mereshchenko, A.N. Tarnovsky, K. Acharya, A. Klinkova, N.N. Hewa-Kasakarage, I. Nemitz, M. Zamkov, Nano Letters 11 (2011) 1792–1799.
[45] T. Risse, S. Shaikhutdinov, N. Nilius, M. Sterrer, H.J. Freund, Accounts of Chemical Research 41 (2008) 949–956.
[46] M.A. Brown, F. Ringleb, Y. Fujimori, M. Sterrer, H.-J. Freund, G. Preda, P. Gianfranco, Journal of Physical Chemistry C 115 (2011) 10114–10124.
[47] M.S. Chen, D.W. Goodman, Science 306 (2004) 252–255.
[48] M. Valden, X. Lai, D.W. Goodman, Science 281 (1998) 1647–1650.